ELSEVIER

Wear 225–229 (1999) 669–677

WEAR

An understanding of the chemical effect on the nano-wear deformation in mono-crystalline silicon components

Liangchi Zhang *, Irena Zarudi

Department of Mechanical and Mechatronic Engineering, The University of Sydney, Sydney, NSW 2006, Australia

Abstract

This paper aims to explain the chemical effect on the wear deformation in mono-crystalline silicon components under nano-sliding. With the aid of various microscopy techniques and theoretical modelling, it shows that two-body and three-body contact sliding processes yield the same mechanism of sub-surface damage. For all the sliding conditions studied with normal loads ranging from 147 mN to 441 mN, no dislocations or micro-cracks were generated. It was found that an amorphous layer always appears and its thickness depends on the sliding load applied and the extent of chemical reaction. Oxygen penetrates into the amorphous layer, changes the atomic bonding of silicon, alters the threshold for amorphous transformation and accelerates wear. However, there still exist a number of problems that need further investigation.

Keywords: Nano-wear; Mono-crystalline silicon; Chemical effect

1. Introduction

The rapid development of modern technologies, such as information technology, has made mono-crystalline silicon a key material in electronic and micro-sliding devices and has necessitated extensive research on its wear behaviour and surface processing methods. A number of studies showed that under smaller loads material removal of samples subjected to two-body abrasion is via ploughing, while under higher loads cutting emerges. No major surface dislocation or phase transformation was developed [1]. Nevertheless, these studies were based on plan-view examinations with a transmission electron microscope (TEM), which cannot monitor the variation of sub-surface structure. More precise investigations showed that amorphous phase transformation during abrasion or indentation does occur [2–10]. The extent of such deformation generated by three-body abrasion depends on the size of slurry particles. When the penetration depths of the particles are on the order of a micron, cracking occurs and brittle fracture dominates the material removal [6]. When the penetration depths of particles/asperities become fractions of a micron, both two-body and three-body contact sliding can lead to a ductile mode of material removal, although dislocation layers beneath amorphous zones, with or without micro-cracks, can also appear [7,8].

A series of theoretical investigations, using molecular dynamics analysis with experimental verification [5,9,10], revealed a more complete picture of nano-wear mechanisms. It was shown that on the nanometre or atomic scale, amorphous phase transformation is the main deformation in mono-crystalline silicon. Under a mechanical abrasion without chemical contamination, the onset of amorphous transformation can be well predicted by a criterion based on the octahedral shearing stress. In a two-body contact sliding, the deformation of silicon falls into the no-wear, adhering, ploughing and cutting regimes, while in three-body contact sliding it follows the regimes of no-wear, condensing, adhering and ploughing. Under certain conditions in three-body sliding, wear without any sub-surface damage can also occur when the bonding strength among surface silicon atoms is weakened chemically and material removal takes place through the mechanism of adhesion. A friction law and a concept for wearability evaluation were thus developed. Although chemical reaction has also been emphasised in the wear of silicon [11,12], the detailed mechanism has not yet been studied carefully.

This paper aims to explore the chemical effect on the nano-wear mechanisms of mono-crystalline silicon components. Various microscopy techniques were used to characterise the sub-surface structure, chemical composition and

* Corresponding author. Tel.: +61-29351-3760; e-mail: zhang@mech.eng.usyd.edu.au

0043-1648/99/$ - see front matter
PII: S0043-1648(98)00378-0

bonding configuration. A statistical model was applied to understand the extent of chemical effects.

2. Experiment

All experiments were conducted on the (100) surfaces of mono-crystalline silicon components. A commercially available Dimple–Grinder (Gatan Model 656/3) was used to generate sliding with $\omega_1 = 420$ rpm and $\omega_2 = 5.4$ rpm, as shown in Fig. 1. The particles used were of α-Al_2O_3 abrasives that have an average diameter of 50 nm with a deviation of 4 nm. These particles were suspended in demineralised double-distilled water and the suspension was added into the sliding zone through a dispenser, see Fig. 1. The size and distribution of particles were examined by a high-resolution scanning electron microscope (HRSEM), JSM-6000F. To obtain a reliable picture of particle size and topography, such as that shown in Fig. 2, the suspension was subjected to ultrasonic agitation for 10 min before sinking them upon a net for HRSEM examination.

The sliding counterpart of the silicon surfaces was a polishing pad of 1 mm in thickness and 15 mm in diameter, made from felt fibres. Its topography was studied by both HRSEM and confocal microscope. To generate reliable data for theoretical investigation, 20 micrographs were analysed. Fig. 3a shows that the surface topography of the pad is dominated by the fibres that are of 8 μm in diameter. However, conglomerations of particles formed during sliding altered the topography to a large extent. An analysis of the surface profile shown in Fig. 3b demonstrates that the asperity heights on the surface with pad-fibres and particle-conglomerations obey a Gaussian distribution, see Fig. 3c, featuring an Rms roughness of 60 μm, standard deviation of surface heights of 31 μm, surface asperity density of 0.16 mm^{-2} and an average asperity radius of 2 μm. However, since the normal sliding loads over the whole contact area were on the order of 100 mN, the typical penetration depth of an asperity into a silicon specimen is on the nanometre scale. Hence, the topography of the pad–particle surface on the finer scale must also be measured. Fig. 3d shows its profile and Fig. 3e demonstrates that it is also described well by a Gaussian distribution, but is now characterised by an Rms roughness of 27 nm, standard deviation of surface heights of 15 nm, surface asperity density of 0.14 nm^{-2} and an average asperity radius of 25 nm.

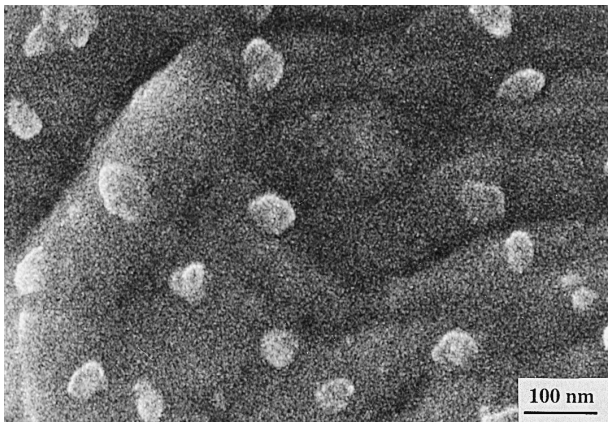

Fig. 2. The α-Al_2O_3 particles after an ultrasonic bath.

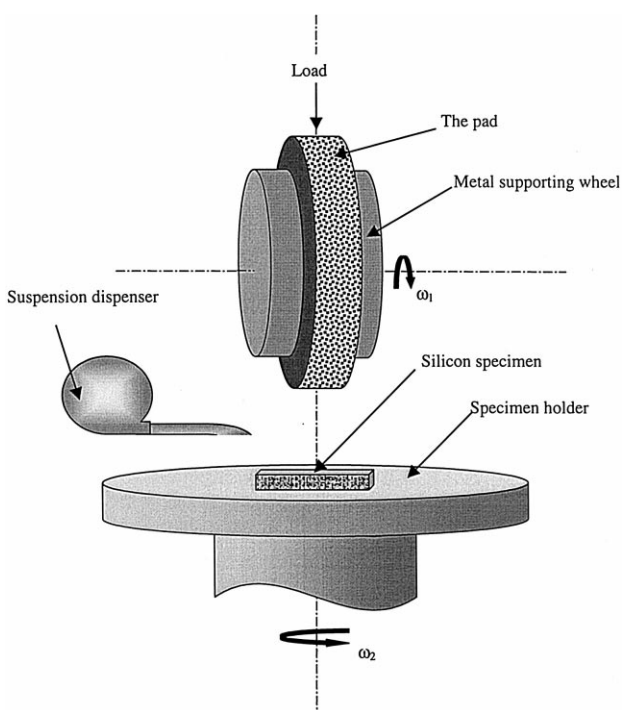

Fig. 1. Schematic diagram of the sliding system.

The elastic modulus of the pad, E_{pad}, was determined by a uniaxial tensile test on an Instron 5567, with an elongation speed of 0.5 mm/min under a wet condition matching its actual sliding environment with that of the suspension. Tests were repeated six times. Poisson's ratio was calculated by measuring the transverse deformation of the pad during elongation, which was done by a video-camera recording system attached to the Instron machine. The magnification used was 100 times.

A silicon specimen was levelled and held at the centre of the specimen holder, see Fig. 1. The duration of each sliding test was 15 min. The normal sliding loads applied were 147 mN, 294 mN and 441 mN, respectively. With the aid of an optical microscope, the wear rates under these loads were determined by measuring the volume removed in sliding and found to be 69 $\mu m^3/s$, 92 $\mu m^3/s$ and 213 $\mu m^3/s$, respectively. The maximum depths of the worn cavities were 2 μm, 2.3 μm and 3.5 μm, correspondingly.

With the above experimental configuration, both two-body and three-body abrasions may occur. When a particle

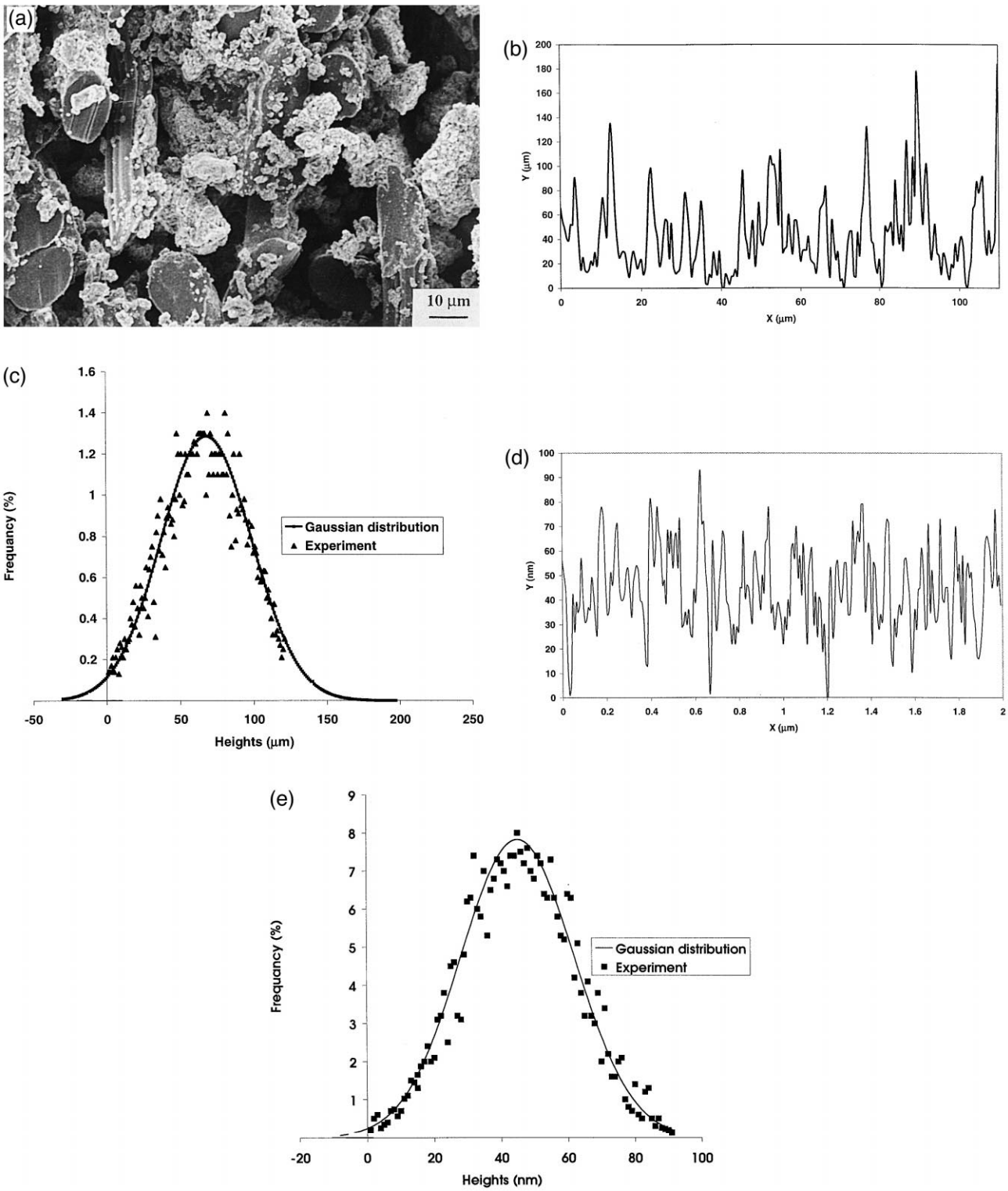

Fig. 3. The surface topography of the pad–particle counterpart. (a) A SEM photo; (b) surface profile on the micron scale; (c) height distribution of the surface on the micron scale; (d) surface profile on the nanometre scale; (e) height distribution of the surface on the nanometre scale.

was held firmly by the pad, a two-body sliding took place. Otherwise, if a particle moved with both translation and rotation, a three-body sliding occurred. Because of the complexity of the pad and particle topography and due to the large number of particles involved, the two sliding processes appeared simultaneously. Individual mechanisms may only be distinguished in some special cases as will be discussed in the later sections.

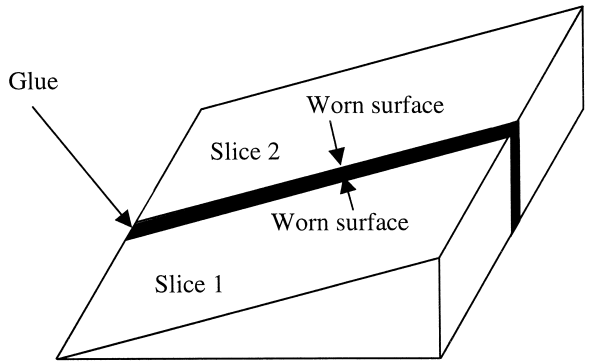

Fig. 4. Cross-section view of wedge-specimens for TEM and STEM investigations.

Surface properties of a worn specimen were investigated by means of atomic force microscopy (AFM). The sub-surface structure was examined by a scanning transmission electron microscope (STEM), VG HB601. As the sub-surface damage zone must be extremely shallow under nano-sliding, cross-section view wedge-specimens, as shown in Fig. 4, rather than the conventional ones with a uniform thickness were used for sub-surface analysis. In the first stage of preparing such specimens, a standard technique described by Ref. [13] was used to make cross-sectional slices. The wedge was made by mechanical and then ion-beam thinning.

A wedge-specimen has a number of advantages over conventional ones. The edge of the former is very thin already and needs only an exposure of 0.5 h in an ion-beam thinner. Artificial effects of ion-beam thinning are minimised. In addition, all analyses under TEM or STEM can be focused on the parts covered by glue so those worn surfaces are not affected during specimen preparation.

Sub-surface structures of worn specimens were studied in high-resolution modes so that the transition of silicon from its initial crystalline structure to an amorphous state could be explored directly. The chemical composition and atomic bonding configuration in sub-surface were determined by electron energy loss spectroscopy (EELS) with a probe diameter of 1 nm.

3. Results and discussion

3.1. Characteristics of worn specimens

Specimens before sliding tests had been made damage-free with Rms surface roughness of 3 nm, as demonstrated in Fig. 5. This insured that sub-surface deformation and micro-structural changes of worn specimens were the result of sliding.

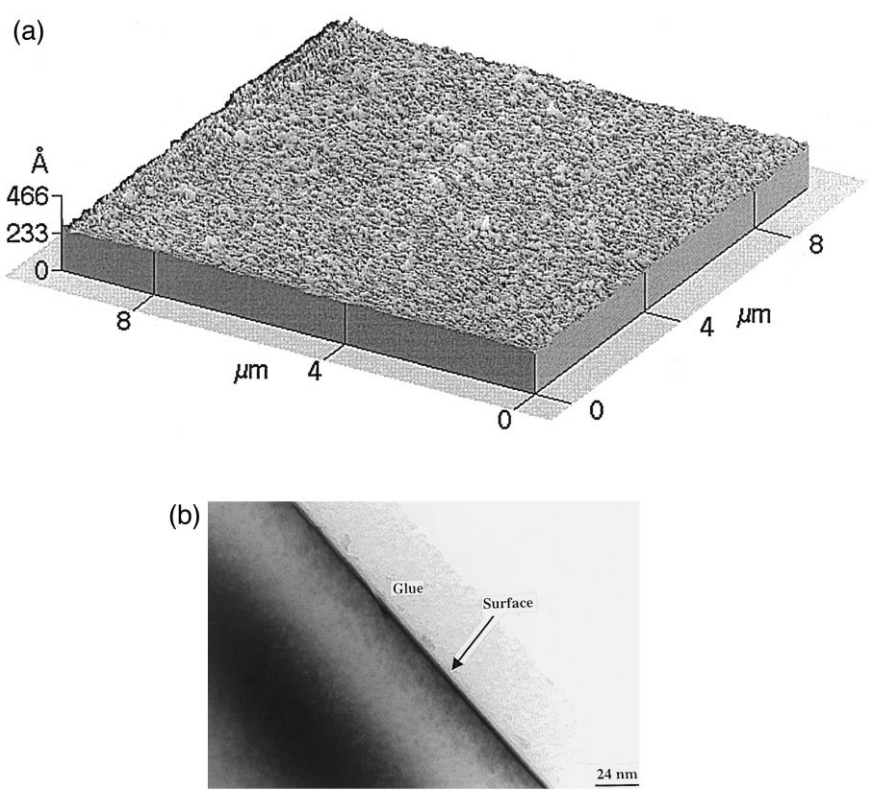

Fig. 5. A silicon specimen before sliding test: (a) surface topography; (b) sub-surface structure.

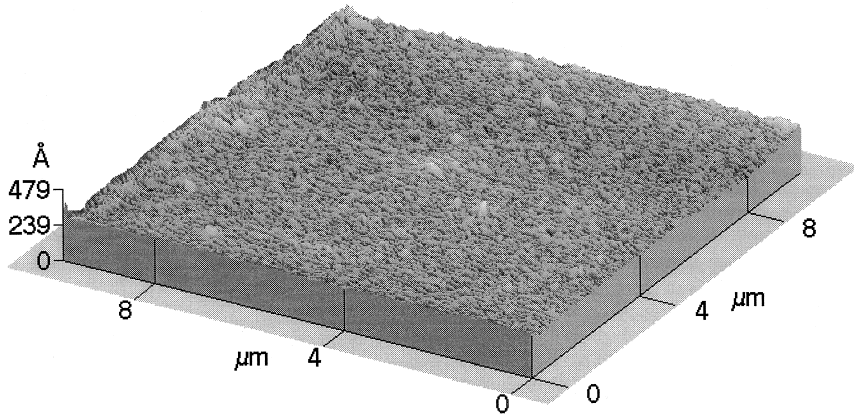

Fig. 6. A typical silicon surface after sliding.

A typical surface topography of worn specimens is shown in Fig. 6. The worn surface is free from micro-fracture but contains some scratches 4 μm to 9 μm wide and up to 20 nm deep (Fig. 7). According to the topographical characterisation of the pad–particle surface, these scratches were produced by conglomerations of particles that were embedded firmly into the pad cavities. This abrasion involved two-body sliding.

Images of the sub-surface at an atomic resolution, Fig. 8, showed that a layer of amorphous silicon always formed during sliding. The layer thickness depended on the normal sliding load applied. Under a load of 441 mN, the thickness of the amorphous layer was 2.7 nm. It decreased with decrease of the load. For instance, under 294 mN and 147 mN, the layer thicknesses became 2.4 nm and 1.3 nm, respectively. Such variation is consistent with what was implied by the criterion recently developed by Zhang and Tanaka [5,9].

No dislocations were activated and no faults were formed, even under the deep scratches (Fig. 7) generated by two-body abrasion. Similar to the findings in diamond–silicon sliding [5] and indentation [9,10], the present results show, once again, that on the nanometre scale deformation via amorphous phase transformation is a more energetically favorable deformation than that via dislocations. Furthermore, the transition from crystalline structure to the amorphous was very smooth and uniform with a transition zone of only three atomic layers, see Fig. 8. The above also indicates that the deformation mechanisms in silicon under two-body and three-body sliding are the same, i.e., they all involve amorphous transformation only.

3.2. Chemical composition change

Two types of atomic bonding configurations were found in the sub-surfaces of all the worn specimens. The bonding configuration in the immediate vicinity of a worn surface

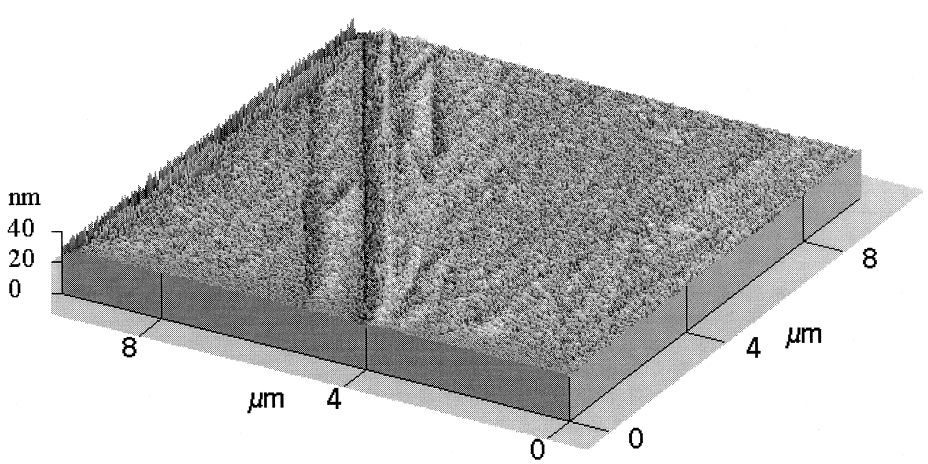

Fig. 7. Scratches generated by two-body abrasion.

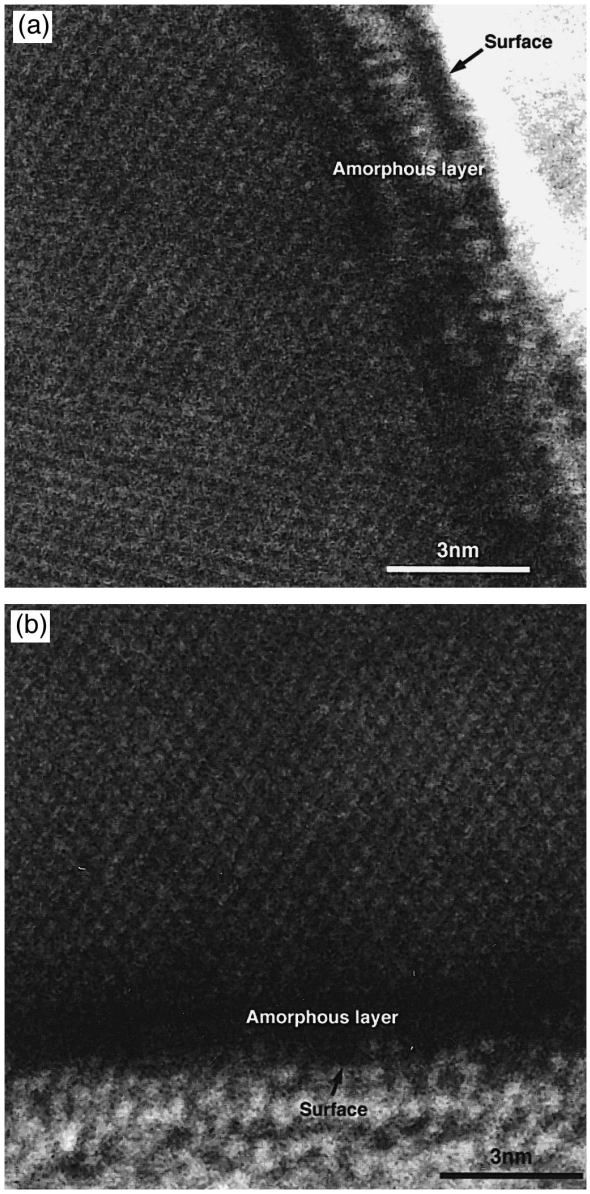

Fig. 8. High-resolution images of sub-surfaces under various normal sliding loads, where each spot represents a silicon atom: (a) 441 mN, (b) 147 mN.

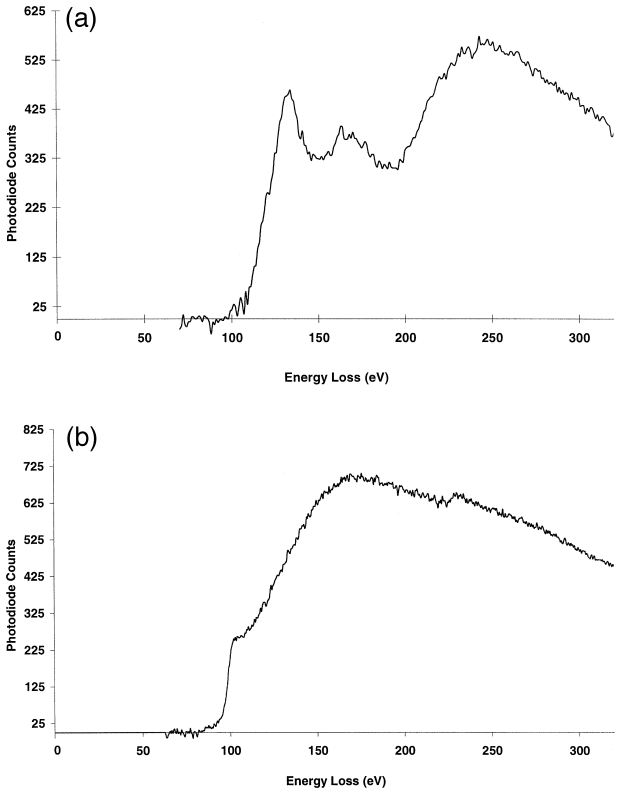

Fig. 9. EELS profiles that reveal bonding configurations in sub-surface after wear: (a) silicon oxide; (b) amorphous silicon.

is characterised by an L-edge at 103 eV, see Fig. 9a, whose profile corresponds to silicon oxide. [1] The material beneath the above zone, which is still within the amorphous layer, has another bonding configuration with an L-edge at 98 eV, see Fig. 9b, whose shape fits the spectra of pure silicon. Hence, sliding not only introduces amorphous transformation but also brings about silicon oxide on the top of the amorphous layer.

Typical examples of oxygen distribution along the sub-surface of worn specimens are shown in Fig. 10, which were obtained by oxygen column scans. In each scanning experiment, 50 spectra were collected along the 8 nm-depth from a worn surface with a beam movement step of 0.16 nm. Although an exact concentration of oxygen cannot be determined by this method, the gradient of oxygen penetration in sub-surface can be seen clearly. [2] The curves show that the penetration depth of oxygen increases with increasing normal sliding load.

3.3. Chemical effect

To find out the extent of the chemical effect on wear deformation during sliding, the mechanical effect without chemical reaction should be understood first. In the present case, it is convenient to examine the thickness variation of the amorphous layer under different loading conditions when chemical factors are excluded. In principle, this can be done by carrying out experiments similar to the above in a contamination-free environment. However, it is practically very difficult and cannot be achieved currently in the authors' laboratory. Thus in this study, a theoretical approach, a stage-wise statistical method, is used to find out the extent of the mechanical effect without chemical reaction.

[1] The EELS used was with a resolution of 0.1 eV.

[2] Since the beam diameter for scanning was 1 nm, the resolution of the method was limited.

Since the Rms surface roughness of a silicon specimen was only 3 nm, its surface can be considered as absolutely smooth compared with its counterpart surface, i.e., the pad–particle surface, that has a Rms roughness of 60 μm. On the other hand, the elastic modulus of silicon, $E_{si} = 159$ GPa, and that of an α-Al_2O_3 particle, $E_{ptl} = 369$ GPa, are much greater than the elastic modulus of the pad, $E_{pad} = 22$ MPa, as will be shown later. It is therefore reasonable to assume, as a first approximation, that α-Al_2O_3 particles are rigid and that the deformation of the sliding system consists of the following two distinct stages under the sliding load.

Stage 1: Micron-scale deformation occurs in the pad only, i.e., no penetration takes place in silicon in this stage.

Stage 2: Nano-scale deformation happens in silicon while the pad deformed in Stage 1 keeps its deformation state unchanged.

Based on the above assumption, a statistical analysis, using the well-known Greenwood–Williamson model [14], is also conducted in two stages. The first deals with the deformation of the pad only that gives rise to the load on each asperity of the pad–particle counterpart, P_1. In the second stage, each pad asperity is considered as a surface with load P_1 and the asperity on such a surface is characterised by the embedded α-Al_2O_3 particles whose topography has been obtained in Section 3.2. [3] By applying the Greenwood–Williamson model again, the load on each α-Al_2O_3 particle, P_2, is determined. The depth of the amorphous zone in the sub-surface of silicon induced by P_2 can then be determined by the criterion of Zhang and Tanaka [5,9], which shows that the threshold of the octahedral shearing stress for the onset of amorphous transformation is 4.6 GPa in the direction [100] or 7.6 GPa in the direction [110]. Since the surface of a silicon specimen was of (100) orientation, the sub-surface cross-section is in the direction [100]. Thus the threshold for the present case is 4.6 GPa.

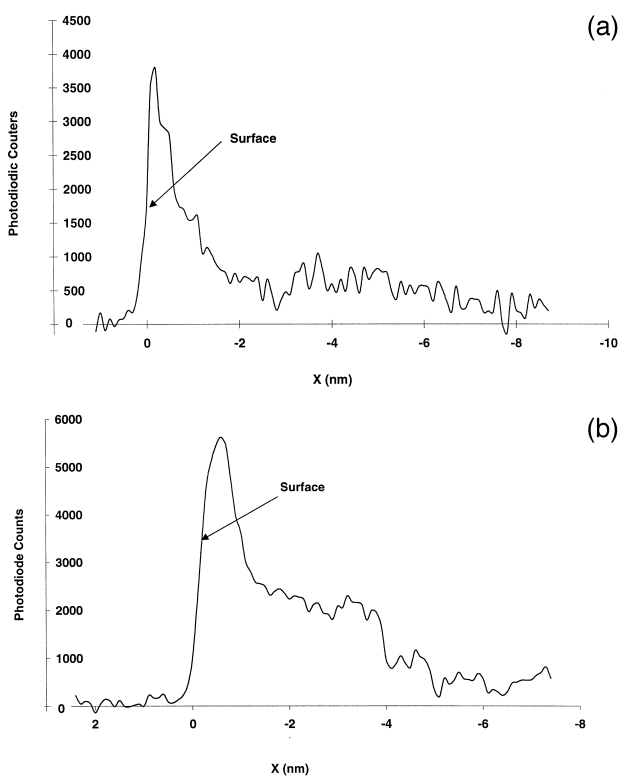

Fig. 10. The variation of oxygen distribution in sub-surface with normal sliding load: (a) sliding load = 147 mN; (b) sliding load = 441 mN. Note that the smaller peaks in deeper sub-surfaces do not mean an increment of oxygen concentration. These were due to some artificial effects such as the thickness increase of the specimen.

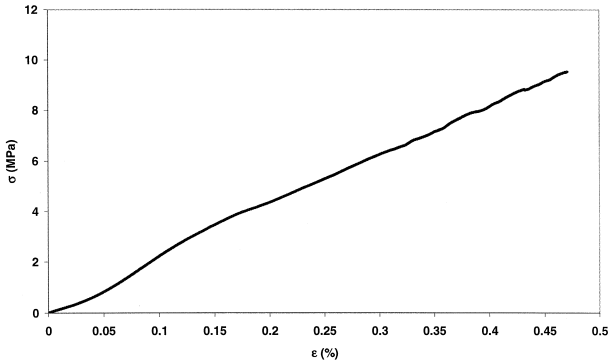

Fig. 11. An example of the stress–strain curves of the pad material.

As reported in Section 3.2, experimental examination shows that sliding under a normal load of 147 mN introduced an amorphous layer of thickness 1.3 nm. Using the above mechanical model, such an amorphous layer can be generated under the same sliding load if the effective modulus of the pad–silicon system, E^*, is 5 MPa. However, when this E^* is used to calculate the thickness of amorphous layer under 294 mN and 441 mN, it leads to 1.55 nm and 1.7 nm, respectively, while the experimental results under these loads were 2.4 nm and 2.7 nm. This means that the mechanical model significantly underestimates the extent of amorphous change and that the actual phase transformation is a much stronger function of the sliding load than the model's indication. On the other hand, if the sliding with 441 mN is used as a reference, a matching prediction by the mechanical model requires $E^* = 35$ MPa. However, this E^* brings about 2.4 nm and 2.3 nm amorphous layers for the cases under loads of 294 mN and 147 mN, respectively. In so doing, the mechanical model greatly overestimates the extent of amorphous change, although once again it underestimates the dependence of amorphous transformation upon the change of the sliding load.

The above inconsistency may be discussed in several ways. First, if amorphous change is introduced mainly by

[3] This is reasonable because, as reported in Section 3.2, the average radius of a pad–particle asperity (2 μm) is 40 times bigger than that of a particle (50 nm).

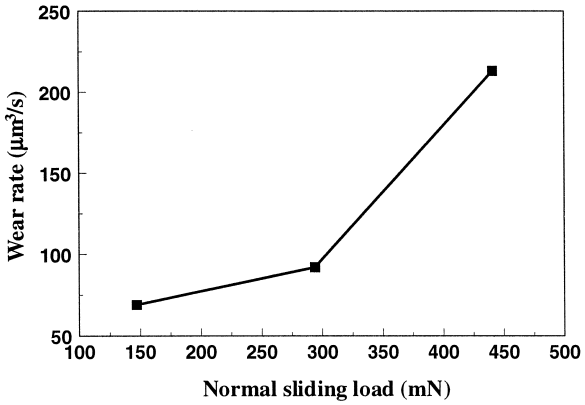

Fig. 12. Variation of wear rate with normal sliding load.

mechanical loading, then the only explanation to the above mismatching between model-prediction and experimental measurement is that the effective modulus of the pad–silicon system must have varied sensitively with the sliding load. In other words, E^* must change from 5 MPa to 35 MPa in a complex manner when the sliding load increases from 147 mN to 441 mN. Unfortunately, this is unlikely since an experimental measurement, such as that shown in Fig. 11, suggests a rather constant Young's modulus and Poisson's ratio. Also, those numbers do not vary significantly from crystalline to amorphous silicon. According to the statistical model, in fact, the increase of the sliding load in the range studied can only change the local contact stresses slightly, and thus cannot alter the extent of amorphous transformation remarkably. All these indicate that there must exist some other factors that also play a dominant role in the amorphous change in addition to the mechanical effect.

One may have realised that deformation in the sliding system happens non-linearly and cannot strictly be divided into the two stages described above. On the other hand, as pointed out by Zhang and Tanaka [5,9], inelastic deformation in silicon emerges instantly when a hard asperity impinges on its surface. In calculating the stress field above, however, it was assumed that the silicon substrate was purely elastic. Thus in reality the occurrence of inelastic deformation around the contact zone with a particle will lower, to a large extent, the level of octahedral shearing stress. Hence, the actual thickness of amorphous layer induced by mechanical loading should be even smaller than those predicted by the above stage-wise model.

When recalling the change of atomic bonding and penetration of oxygen into the amorphous zone during sliding, as reported in Section 3.2, the most appropriate explanation for the discrepancy between the mechanical prediction and experimental measurement is the chemical reaction during sliding. A recent study [11] showed that the penetration of oxygen into the sub-surface is enhanced by the tensile stress field associated with mechanical loading and controlled by the diffusion coefficient of oxygen. In the present case, the authors believe that the chemical reaction alters the microstructure of the material and changes the threshold of transformation from crystalline to amorphous. Under a smaller load, e.g., 147 mN, the pad was deformed less and thus the number of active asperities per unit time during sliding was also less. Under a larger load, e.g., 441 mN, however, this number became 2.84 times greater. Every time an asperity–silicon interaction occurred it 'pushed' oxygen into the silicon sub-surface, accelerated by its tensile stress field generated. Since the 'pushing' frequency was 2.84 times higher in the case of 441 mN, the thickness of the amorphous layer accelerated by the chemical reaction, 2.7 nm, must be larger than that predicted by the mechanical model, 1.7 nm. Similarly, the high interaction frequency under higher loads also accelerated the wear rate of silicon, as shown in Fig. 12.

4. Conclusions

The above investigation brings about the following conclusions.

(1) Chemical reaction during sliding plays an important role in the nano-wear deformation of a mono-crystalline silicon component. The effect is through the change of atomic bonding in the amorphous layer. The increase of the normal sliding load enhances greatly the chemical effect and increases the wear rate.

(2) Dislocations do not appear in a mono-crystalline silicon subjected to nano-sliding. This is consistent with the molecular dynamics analysis.

(3) Although the present investigation has qualitatively described the mechanisms involved in the sub-surface deformation, further studies are necessary to find out exactly the rate of oxygen penetration, the origin of threshold change due to chemical reaction, and their quantitative effect on wear rate. To understand more precisely the mechanical effect via theoretical modelling, a reliable characterisation method for the pad material must be developed.

Acknowledgements

The authors wish to thank the Australian Research Council for its continuous support of this project. The Electron Microscope Unit of Sydney University offered free access to its facilities.

References

[1] V.N. Koinkar, B. Bhushan, J. Mater. Res. 12 (1997) 3219–3224.
[2] G.M. Pharr, W.C. Oliver, D.S. Harding, J. Mater. Res. 6 (1991) 1129–1130.
[3] D.L. Callahan, J.C. Morris, J. Mater. Res. 7 (1992) 1614–1617.
[4] G.M. Pharr, W.C. Oliver, F.R. Brotzen, J. Mater. Res. 7 (1992) 613–617.
[5] L. Zhang, H. Tanaka, Atomic scale deformation in silicon mono-

crystals induced by two-body and three-body contact sliding, Tribology International, 1998, in press.
[6] Zarudi, L. Zhang, J. Mater. Sci. Lett. 15 (1996) 586–587.
[7] Zarudi, L. Zhang, J. Mater. Pros. Tech., 1998, in press.
[8] L. Zhang, H. Tanaka, I. Zarudi, Procs. 12th ASPE Conf., 1997, 462–465.
[9] L. Zhang, H. Tanaka, On the mechanics and physics in the nano-indentation of silicon mono-crystals, JSME International, Series A, under review.
[10] H. Tanaka, L. Zhang, in: L. Zhang, N. Yasunaga (Eds.), Advances in Abrasive Technology, World Scientific, 1997, 43–47.
[11] L.M. Cook, J. Non-Cryst. Sol. 120 (1990) 152–171.
[12] K. Tkácova, N. Ševulová, Z. Bastl, P. Stopka, M. Bálintová, J. Mater. Res. 10 (1995) 2728–2735.
[13] Zarudi, L. Zhang, Y.-W. Mai, J. Mater. Sci. 33 (1996) 905–914.
[14] J.A. Greenwood, J.B.P. Williamson, Proc. R. Soc. London 295 (1966) 300–319.